2023 62nd IEEE Conference on Decision and Control (CDC)
December 13-15, 2023. Marina Bay Sands, Singapore

Economic Dispatch for DC Microgrids: An Optimal Power Sharing Approach with Batteries

Armin Gießler, Pol Jané-Soneira, Albertus Johannes Malan and Sören Hohmann

Abstract— **In this paper, we propose a hierarchical control structure comprising three layers which is able to (i) achieve economic dispatch for islanded DC microgrids, (ii) compensate load and generation disturbances with batteries performing power sharing and (iii) stabilize non-passive constant power loads. The batteries are charged economically optimally by the third layer controller such the state of charges (SOCs) remain constant. The proportional power sharing of the batteries is achieved by employing a novel control law which solves the linearized steady-state power flow equations in real time. The microgrid is stabilized by using voltage controllers for batteries and active damping elements. A numeric method to verify closed-loop asymptotic stability is derived. The power sharing of the batteries and stability achieved with the proposed control is demonstrated in a simulation.**

I. Introduction

Driven by environmental concerns, power systems are undergoing a major transformation towards the integration of more and more volatile renewable energy sources (RESs), such as photovoltaic and wind generation units. The rapid deployment of these distributed generation units (DGU) creates two challenges: the volatility of energy supply and the low inertia in emerging power grids [1], e.g. in DC microgrids. This can lead to instabilities in the power grid and economic inefficiencies. Microgrids have been postulated as a conceptual solution to overcome these challenges by using advanced control methods to coordinate DGUs, storages and loads [2], [3]. In order to withstand the power balance deviations due to load and generation prediction errors, a resilient control method is needed which utilizes storage units, e.g. batteries, flexible loads or emergency reserves.

Literature review: Using an energy management systems (EMS) is a common approach to achieve optimal resource scheduling [4]–[6]. The EMS optimizes an objective over a discrete control horizon by using generation and load predictions to obtain the optimal scheduling for the next time step. The power flow equation and technical constraints are considered in the optimization problem. Furthermore, energy storages within the power grid improve its flexibility, economic efficiency and reliability by compensating the volatile energy production of RESs [7], [8]. Typically, the EMS generates the optimal scheduling with the assumption that all loads and generators consume and inject constant power over a period of time.

It is known that constant power (P) loads can be responsible for voltage oscillations leading to instability within the microgrid [9]–[12]. Therefore, it is questionable whether EMSs can be directly applied to real world microgrids. In [9], [10], the authors present a plug-and-play approach based on passivity to stabilize any type of load. The proposed voltage controllers ensure strict passivity for every type of load. However, these works do not include any economic consideration. In [13], the authors present a hierarchical control architecture comprising three layers which combines an EMS and stabilizing voltage controllers. However, only passive ZIP (constant impedance, constant current, and constant power) loads are considered and the EMS neglect network losses. Furthermore, prediction errors or disturbances can lead to a loss of economic optimality.

Proportional power sharing is a common objective in microgrids which allows generators to counteract disturbances cooperatively (see e.g. [14]–[16]). The authors of [15], [16] achieve power sharing by considering a highly simplified dynamic model of a microgrid, e.g. the time derivative of the power flow equations or just the resistive part of the microgrid. In [14], the authors postulate a four-stage distributed controller which achieves power sharing by using a realistic dynamic model for DGUs and transmission lines. However, no economic consideration is made and no interface to the EMS is provided.

Contributions: We propose a three layer control architecture which achieves economic dispatch within the microgrid while compensating load and generation imbalances by proportional power sharing among batteries. The main contributions of the paper at hand are:

1) The three layer controller which ensures the exact scheduling for optimal power flow (OPF) to a realistic dynamic model of an islanded DC microgrid. The OPF problem is extended to charge the batteries in an economically optimal fashion since the work performed by batteries, e.g. the change in SOCs, is considered.
2) The second layer which counteracts the suboptimal economics arising from load and generation disturbances not considered in DC-OPF. This is achieved through proportional power sharing among the batteries, with a novel real-time control law based on a linearized version of the power flow equation.
3) The first layer which stabilizes nonpassive P-loads and P-generators with batteries and active damping elements. Sufficient conditions for closed-loop asymptotic stability are derived.

A. Gießler, P. Jané-Soneira, A. J. Malan, S. Hohmann are with the Institute of Control Systems, Karlsruhe Insitute of Technology (KIT), 76131, Karlsruhe, Germany. Corresponding author is Armin Gießler, armin.giessler@kit.edu.

979-8-3503-0123-6/23/$31.00 ©2023 IEEE

Paper Organisation: The introduction ends with some notation and preliminaries on power grids as graphs and on DC-OPF. In Section II, we present the modelling of the DC microgrid and the architecture as well as the design of our three layer controller. Next, we derive sufficient numerical conditions for closed-loop asymptotically stability in Section III. Finally, in Section IV, we demonstrate the asymptotic stability of the closed loop and the power sharing among the batteries. The paper ends with a conclusion in Section V.

Notation: The set of (strictly positive) real numbers is denoted by $\mathbb{R}$ ($\mathbb{R}^+$). The transpose of a matrix A (a vector B) is denoted by A^T (B^T). A symmetric positive definite (semi-definite) matrix A is denoted by $A > 0$ ($A \geq 0$). The operator $\circ$ stands for the Hadamard Product. The diagonal matrix of the vector x is denoted by $\text{diag}(x)$. The k-dimensional vector of ones (zeros) is defined as 1_k (0_k). The identity matrix with dimension k is denoted by $\mathbf{I}_k$ and $\mathbf{0}_{k\times n}$ represents a $k \times n$ matrix filled with zeros. A directed graph is denoted by $\mathcal{G}(\mathcal{N}, \mathcal{E})$, where $\mathcal{V}$ and $\mathcal{E} \subseteq \mathcal{N} \times \mathcal{N}$ are the sets of nodes and edges, respectively. The set $\mathcal{N}_i$ denotes the set of neighboring nodes of node $i \in \mathcal{N}$ or edge $i \in \mathcal{E}$.

A. Preliminaries

1) Power Grids as Graphs: The topology of power grids can be modelled as a directed graph $\mathcal{G}(\mathcal{N}, \mathcal{E})$ in which nodes represent the buses and edges represent the transmission lines. The set of buses is defined as $\mathcal{N} = \{1, \ldots, N\}$ and the set of edges as $\mathcal{E} = \{1, \ldots, M\}$. The direction of the edges of the directed graph is arbitrarily chosen and determines the positive current direction over the line. The incidence matrix $B \in \{-1, 0, 1\}^{N\times M}$ of a directed graph is defined as $B = (B_{ij})$ with $B_{ij} = -1$ if $(i, j) \in \mathcal{E}$, $B_{ij} = 1$ if $(j, i) \in \mathcal{E}$ and $B_{ij} = 0$ otherwise. The nodal admittance matrix $Y \in \mathbb{R}^{N\times N}$ of a DC power grid can be calculated by $Y = B\text{diag}(Y_l)B^T$, where $Y_l = [Y_{l1}, \ldots, Y_{lM}]^T$ denotes the transmission line conductances for which the entries of Y_l are in the same order as the columns of B [17, Eq. (1)].

2) DC-OPF: In this work, the economic dispatch OPF problem is considered, in which the cost of the total power generation is minimized subject to the given loads and technical constraints [18]. Using Kirchhoff's laws, the power flow equation in Bus $i \in \mathcal{N}$ can be obtained and is described by

$$P_i = P_i^G - P_i^L = \sum_{j\in\mathcal{N}_i} Y_{ij}(V_i^2 - V_i V_j), \tag{1}$$

where P_i is net power injection at Bus i, $P_i^G \geq 0$ is the generated power flowing into Bus i, $P_i^L \geq 0$ is the demand power flowing out of the Bus i, and V_i and V_j are the voltages at Bus i and j, respectively. The power flow equations (1) of the power grid can be written in network variables [18, Eq. 32]

$$P = P^G - P^L = V \circ YV, \tag{2}$$

where $P = [P_1, \ldots, P_N]^T$, and P^G, P^L and V are defined equivalently.

Definition 1: The economic dispatch DC-OPF problem is defined by the following optimization problem:

$$\begin{aligned}
\min_{P^G,V} \; & \sum_{i\in\mathcal{N}} c_i(P_i^G) \\
\text{s.t. } & P^G - P^L = V \circ YV \\
& 0 < V_{\min} \leq V_i \leq V_{\max} \quad \forall i \in \mathcal{N} \setminus \{1\} \\
& V_1 = V_{\text{ref}}^* \\
& 0 \leq P_i^G \quad \forall i \in \mathcal{N},
\end{aligned}$$

where $c_i(P_i^G) : \mathbb{R}^+ \rightarrow \mathbb{R}$ describes an assumed monotonically increasing cost function of the generator of Bus i and Bus 1 represents a slack bus with predefined voltage V_{ref}^*.

II. Modelling and Controller Design

In this section, we describe the microgrid as well as the hierarchical control architecture in Subsection II-A and the three layers of the controller in Subsections II-B to II-D.

A. Microgrid and Hierarchical Control Architecture

We consider islanded DC microgrids with a topology described by a directed graph $\mathcal{G} = (\mathcal{N}, \mathcal{E})$.

Assumption 1: The set of buses $\mathcal{N}$ is partitioned into two sets $\mathcal{N}_B = \{1, \ldots, N_B\}$ and $\mathcal{N}_D = \{N_B + 1, \ldots, N_B + N_D\}$, where $\mathcal{N} = \mathcal{N}_B \cup \mathcal{N}_D$ and $\mathcal{N}_B \cap \mathcal{N}_D = \emptyset$. The sets $\mathcal{N}_B$ and $\mathcal{N}_D$ represent buses with batteries and damping elements, respectively.

The buses $\mathcal{N}_B$ contain a battery with a state-feedback controller which tracks the bus voltage to a reference voltage whereas the buses $\mathcal{N}_D$ contain a damping element which improves the overall grid stability. Both types of buses can additionally contain a constant power generator and/or a constant power load. In the following, these are abbreviated as P-generator P^G and P-load P^L and are summarized as P-injection $P = P^G - P^L$ as in (2). In order to keep the bus voltages inside the feasible region $V_{\min} \leq V_i \leq V_{\max}$, Bus 1 represents a slack bus and is responsible for forming the voltage levels in the microgrid.

The hierarchical control architecture contains three layers as shown in Fig. 1. The third and highest layer contains the

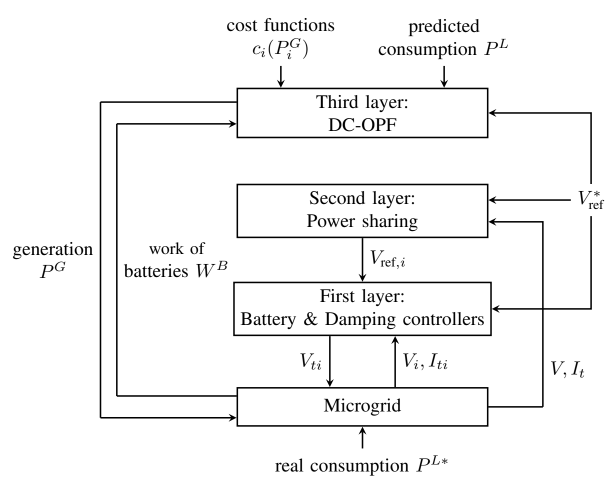

Fig. 1. Control architecture and structure of the closed-loop system

DC-OPF which generates an economically optimal scheduling of the generators in discrete time steps. This layer gets the predicted power demands at each node P^L and the measurements of the work performed by the batteries W^B, e.g. the change of the state of charge (SOC) of the batteries. To ensure robustness against load and generation disturbances, it is desirable to keep the batteries at a constant SOC between 0% and 100%. Thus, the third layer controller recharges or discharges the batteries in the next time step depending on the work performed by batteries. The second layer is independent of the third layer and compensates any disturbances that the third layer has not considered within the current time step. For this purpose, the controller of the second layer generates reference voltages V_{ref} in real time for the state-feedback controllers of the batteries such that proportional power sharing is achieved. The first layer contains voltage controllers for the batteries and the active damping elements to track the bus voltages to the reference voltages and stabilize P-injections. The physical DC microgrid interacts with all three layers by providing measurements of bus voltages V, filter currents I_t and performed work of the batteries W^B and receiving generations P^G and voltages references V_{ref} for the voltage sources V_t. There are two control loops in Fig. 1: a discrete-time loop between the third layer and the microgrid and a continuous-time loop between the first and second layers and the microgrid. All three layers and the microgrid components are explained in the following three subsections.

B. First Layer Controller and Microgrid Elements

In this subsection, the microgrid elements: batteries, damping elements and transmission lines, and the voltage controllers are explained. The first layer controller comprises the local voltage controllers of the batteries and the damping elements which track the bus voltages $V_i, i \in \mathcal{N}_B$ to the reference voltages V_{ref} and improve the stability of the microgrid.

1) Transmission line: Transmission lines are modelled with the π-equivalent model [19, Subsec. 3.1.1]. The line capacitances $\frac{C_l}{2}$ are grouped with the filter capacitance C_{fi} as in [12] and the sum of capacitance is denoted by $C_{ti} = C_{fi} + \frac{C_l}{2}$ (see Fig. 2). At every bus, there is a filter capacitance because of Assumption 1. The dynamics of a power line $l \in \mathcal{E}$ is described by [12, Eq. (11)]

$$\dot{I}_l = -\frac{R_l}{L_l} I_l + \sum_{i \in \mathcal{N}_l} B_{il} V_i, \tag{3}$$

where $R_l > 0$ denotes the line resistance and $L_l > 0$ denotes the line inductance.

2) Battery with or without P-injection: The battery is modelled as a controllable voltage source and a series RLC filter (see Fig. 2). The net P-injection P_i^* by the P-generators and/or P-loads at Bus i are modelled as an ideal current source with $I_{P,i} = P_i^*/V_i$. The predicted P-injections P in the third layer are denoted without the star (see (2)). The battery voltage V_{ti} is controlled by the state-feedback controller from [11] which allows the bus voltage V_i track

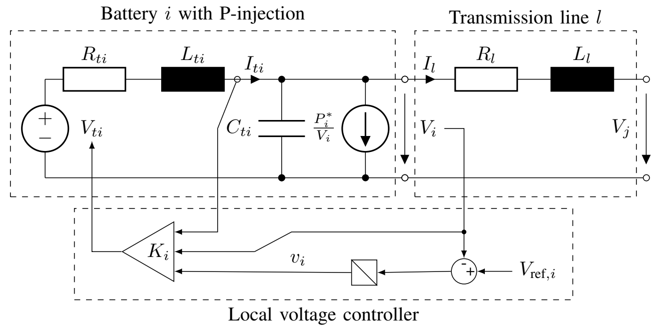

Fig. 2. Circuit diagram of the battery with P-injection and local voltage controller at Bus i, and transmission line l [12, Fig. 3]

the reference voltage $V_{\mathrm{ref},i}$ provided by the second layer controller. To this end, an integrator state $\dot{v}_i = V_{\mathrm{ref},i} - V_i$ is introduced, yielding the controller

$$V_{ti} = K_i x_i = \begin{bmatrix} k_{1,i} & k_{2,i} & k_{3,i} \end{bmatrix} \begin{bmatrix} V_i & I_{ti} & v_i \end{bmatrix}^T,$$

where $x_i = [V_i, I_{ti}, v_i] \in \mathbb{R}^3$ is the state of the Bus $i \in \mathcal{N}_B$ and $k_{1,i}, k_{2,i}, k_{3,i} \in \mathbb{R}^+$ are control parameters. The dynamics of the closed-loop subsystem consisting of the battery and the P-injection is given by

$$\begin{bmatrix} \dot{V}_i \\ \dot{I}_{ti} \\ \dot{v}_i \end{bmatrix} = \begin{bmatrix} \frac{1}{C_{ti}} I_{ti} + \frac{1}{C_{ti}} V_i^{-1} P_i^* - \frac{1}{C_{ti}} I_i \\ \alpha_i V_i + \beta_i I_{ti} + \gamma_i v_i \\ -V_i + V_{\mathrm{ref},i} \end{bmatrix}, \tag{4}$$

where $\alpha_i = \frac{1}{L_{ti}}(k_{1,i} - 1), \beta_i = \frac{1}{L_{ti}}(k_{2,i} - R_{ti})$ and $\gamma_i = \frac{1}{L_{ti}} k_{3,i}$.

3) Damping Element with P-injection: Inspired by the robust passifying voltage controller in [10, Theorem 3], we propose an active damping element which comprising a voltage source and a series RLC filter (see Fig. 3) to counteract the voltage destabilizing effects of P-loads. Damping is achieved through a state-feedback controller that utilizes two additional states. The state e_i adds damping to the filter current I_{ti} which counteracts fast changes in the bus voltage V_i and increase overall grid stability. The state q_i

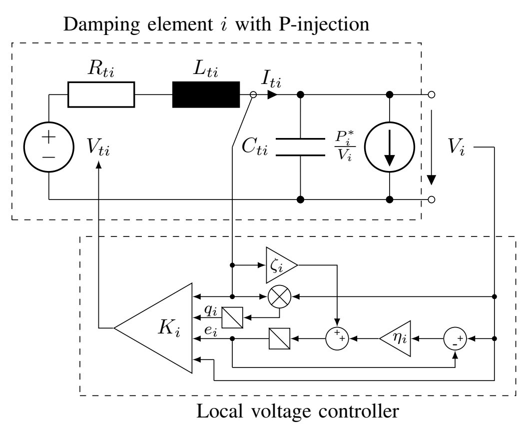

Fig. 3. Circuit diagram of the damping element with P-injection and local voltage controller at Bus i

with nonlinear dynamics represents the overall work of the damping element $W_i^D = \int_{t_0}^{\infty} V_i I_{t,i} \mathrm{d}t$. Negative feedback on q_i is introduced with the aim of damping the work W_i^D to zero. The linear state-feedback control law is given by

$$\begin{aligned} V_{ti} &= K_i x_i \\ &= \begin{bmatrix} 1-k_{2,i} & -k_{1,i} & k_{1,i} & -k_{3,i} \end{bmatrix} \begin{bmatrix} V_i & I_{ti} & e_i & q_i \end{bmatrix}^T, \end{aligned}$$

where $k_{1,i}, k_{2,i}, k_{3,i} \in \mathbb{R}^+$ are control parameters. The dynamics of the closed-loop system consisting of the damping element and the P-injection are given by

$$\begin{bmatrix} \dot{V}_i \\ \dot{I}_{ti} \\ \dot{e}_i \\ \dot{q}_i \end{bmatrix} = \begin{bmatrix} \frac{1}{C_{ti}} I_{ti} + \frac{P_i^*}{C_{ti} V_i} - \frac{1}{C_{ti}} I_i \\ \alpha_i V_i + \beta_i I_{ti} + \delta_i e_i + \varepsilon_i q_i \\ \zeta_i I_{ti} + \eta_i (V_i - e_i) \\ V_i I_{ti} \end{bmatrix}, \tag{5}$$

where $\alpha_i = -\frac{1}{L_{ti}} k_{2,i}, \beta_i = \frac{1}{L_{ti}}(-R - k_{1,i}), \delta_i = \frac{1}{L_{ti}} k_{2,i}, \varepsilon_i = -\frac{1}{L_{ti}} k_{3,i}, \zeta_i = \tau_i k_{1,i}$ and $\eta_i = \tau_i k_{2,i}$. The time constant $\tau > 0$ is a tuning factor.

C. Second Layer Controller

The second layer controller solves a linearized version of the power flow equation (2) in real-time and generates voltage references V_{ref} for the first layer controller such that the desired power sharing among the batteries is achieved.

Lemma 1: The derivative $J_P : \mathbb{R}^{N \times N} \to \mathbb{R}^N$ of the power flow equations (2) with respect to the voltages V is given by

$$J_P(V) = \frac{\partial}{\partial V} P = \mathrm{diag}(V) Y + \mathrm{diag}(YV). \tag{6}$$

Proof: The power flow equations can be rewritten as

$$\begin{aligned} P &= V \circ YV = YV \circ V \\ &= \mathrm{diag}(V) YV = \mathrm{diag}(YV) V. \end{aligned} \tag{7}$$

Applying the product rule to (7) results in

$$J_P(V) = V \circ \frac{\partial}{\partial V}(YV) + YV \circ \frac{\partial}{\partial V}(V),$$

which directly yields the result in (6). ■

Definition 2: The real-time control law of the second layer controller is defined by the voltage reference $V_{\text{ref}}(V, I_t) : \mathbb{R}^N \times \mathbb{R}^N \to \mathbb{R}^{N_B}$,

$$V_{\text{ref}}(V, I_t) = \begin{bmatrix} V_{\text{ref}}^* \\ \begin{bmatrix} \mathbf{0}_{N_B-1 \times 1} & \mathbf{I}_{N_B-1} & \mathbf{0}_{N_B-1 \times N_D} \end{bmatrix} Z \end{bmatrix} \text{ with} \tag{8}$$

$$\begin{aligned} Z = &\begin{bmatrix} -F & J_{P,2:N}(V) \end{bmatrix}^{-1} \\ &\cdot \left(-\mathrm{diag}(I_t) V - J_P(V) \left(\begin{bmatrix} V_{\text{ref}}^* \\ 0_{N-1} \end{bmatrix} - V \right) \right), \end{aligned} \tag{9}$$

where V_{ref}^* denotes the time-invariant slack bus voltage, $F = \begin{bmatrix} F_1 & \dots & F_{N_B} & 0_{N_D}^T \end{bmatrix}^T, F_i \in \mathbb{R}^+ \cup \{0\}$ for $i \in \mathcal{N}_B$ represents a weighting vector and $J_{P,2:N}$ denotes the second to the last columns of the Jacobian matrix J_P (6).

Theorem 1: The control law of Definition 2 compensates load and generation disturbances while achieving exact power sharing of all batteries at steady state. Proportional power sharing of the batteries is realized by choosing different weighting factors F_i for $i \in \mathcal{N}_B$.

Proof: We derive the control law of Definition 2 by solving the linearized power flow equation with desired proportional power sharing. The net power injection of all buses P can be calculated out of voltages V by

$$P = V \circ YV = P^P + P^{B,D} = P^P + \mathrm{diag}(I_t) V \tag{10}$$

which we partition into two parts, the injection by P-loads and P-generators $P^P = P^G - P^L$, and the injections by batteries and damping elements $P^{B,D}$. The linearized power flow equation around the operation point V are given by

$$\begin{aligned} P' &= P + \frac{\partial}{\partial V'} (V' \circ YV') \Big|_{V'=V} (V' - V) \\ &= P + J_P(V)(V' - V), \end{aligned} \tag{11}$$

where $J_P(V)$ can be directly calculated by using Lemma 1. Equation (11) is solved with respect to the voltages V' such the power $P^{B,D}$ is provided by proportional power sharing among the batteries $F P_{\text{bat}}$, where $P_{\text{bat}} \in \mathbb{R}$ represents a power which is scaled by the weighting vector F. From the linear system of equations (11) with $P' = P^P + F P_{\text{bat}}$, $V' = [V_{\text{ref}}^*, V_2', \dots, V_N']$ and (10), the vector $Z = \begin{bmatrix} P_{\text{bat}}, V_2', \dots, V_N' \end{bmatrix}^T$ can be obtained through matrix manipulations:

$$P^P + F P_{\text{bat}} = P^P + \mathrm{diag}(I_t) V + J_P(V) \begin{bmatrix} V_{\text{ref}}^* - V_1 \\ V_2' - V_2 \\ \vdots \\ V_N' - V_N \end{bmatrix} \tag{12}$$

$$\begin{aligned} \Leftrightarrow -\mathrm{diag}(I_t) V - J_P(V) \begin{bmatrix} V_{\text{ref}}^* - V_1 \\ -V_2 \\ \vdots \\ -V_N \end{bmatrix} &= J_P(V) \begin{bmatrix} 0 \\ V_2' \\ \vdots \\ V_N' \end{bmatrix} - F P_{\text{bat}} \\ &= \begin{bmatrix} -F & J_{P,2:N}(V) \end{bmatrix} Z, \end{aligned}$$

which directly yields (9). The reference vector for the controllers of the batteries $V_{\text{ref}}(V, I_t) = \begin{bmatrix} V_{\text{ref}}^* & V_2' & \dots & V_{N_B}' \end{bmatrix}^T$ can be calculated by (8). The error of the linearization of the power flow equations (11) is zero at steady state because of the permanent linearization around the operating point V. Combined with the desired proportional power sharing in (12), the voltage reference V_{ref} achieves exact proportional power sharing in steady state. ■

Remark 1: In order to obtain a unique solution to the linear system of equations (12), it is necessary to have exactly one slack bus with voltage reference V_{ref}^*. This balances the unknown variables with the number of equations in (12).

Remark 2: The weighting vector F of Theorem 1 can be chosen such that the entries correspond to the costs of the energy of the two batteries. This way, disturbances of the P-injections can be compensated economically optimal.

Because the control law of Theorem 1 does not consider voltage constraints, e.g. $V_{\min} \le V_i \le V_{\max}$, the following assumption is made.

Assumption 2: The disturbances of loads and generators are sufficiently small such that the applied reference voltages

V_{ref} by Theorem 1 generate feasible voltage trajectories with $V_{\min} \leq V_i \leq V_{\max}$ for all $i \in \mathcal{N}$ and $t \in \mathbb{R}^+$.

Remark 3: Even though the control law (9) is provided in real-time, exact power sharing cannot be guaranteed in the transient case, because the dynamics of the microgrid are not considered.

The control law (9) includes an inversion of the time-variant matrix $\begin{bmatrix} F & J_{P,2:N} \end{bmatrix} \in \mathbb{R}^{N \times N}$, which may be computationally expensive for large power grids. Therefore, we provide a linearized time-invariant version of the controller in Definition 2.

Definition 3: The linearized control law $V_{\text{ref}}(V, I_t)$ of Definition 2 around the operation point $(V_0, I_{t,0})$ is defined as

$$\begin{aligned} V_{\text{ref,lin}}(V, I_t) &= V_{\text{ref}}(V_0, I_{t,0}) + \frac{\partial}{\partial V} V_{\text{ref}}(V, I_t)\bigg|_{\substack{V=V_0 \\ I_t=I_{t,0}}} (V - V_0) \\ &\quad + \frac{\partial}{\partial I_t} V_{\text{ref}}(V, I_t)\bigg|_{\substack{V=V_0 \\ I_t=I_{t,0}}} (I_t - I_{t,0}) \\ &= G_0 + G_1 V + G_2 I_t, \end{aligned} \tag{13}$$

where $G_0 \in \mathbb{R}^{N_B}$ represents a constant offset and $G_1, G_2 \in \mathbb{R}^{N_B \times N}$ are the gains for the feedback of voltages V and filter currents I_t.

Even though the linearized control law of Definition 3 cannot be stated explicitly for systems of arbitrary dimension, it does provide a time-invariant, closed form control law which can be easily obtained for smaller microgrids.

Remark 4: The time-invariant control law of Definition 3 achieves in general approximate proportional power sharing among the batteries, since there is a linearization error at steady state if the steady-state states (V, I_t) are different to $(V_0, I_{t,0})$.

D. Third Layer Controller

The third layer controller solves the economic dispatch DC-OPF (see Definition 1) with a finite control horizon $k_{\max} \geq 1$ and sampling time $T \in \mathbb{R}^+$. It receives predictions of the loads $P^L(k)$ for all time steps $k \in \mathcal{K} = \{k_0, \dots, k_0 + k_{\max} - 1\}$ of the control horizon, where k_0 is the current time step. Furthermore, the controller receives the work $W^B = [W_1^B, \dots, W_{N_B}^B, 0_{N_D}^T]$ done by the batteries within the last sampling period. In order to charge or discharge the batteries such that its SOCs are kept at a constant value, $P^B = \frac{1}{T} W^B$ is added on the left side of the power flow equations (2) during the first time step k_0. Hence, the third layer controller injects the correct amount of power such that the SOCs remain constant. The third layer controller solves at every time step the following optimization problem

$$\begin{aligned} \min_{P^G(k), V(k)} \; & \sum_{k \in \mathcal{K}} \sum_{i \in \mathcal{N}} c_i(P_i^G(k)) \\ \text{s.t. } & P^G(k_0) - P^L(k_0) - P^B = V(k_0) \circ YV(k_0) \\ & P^G(k) - P^L(k) = V(k) \circ YV(k) \quad \forall k \in \mathcal{K} \setminus \{k_0\} \\ & 0 < V_{\min} \leq V_i(k) \leq V_{\max} \quad \forall i \in \mathcal{N} \setminus \{1\} \\ & V_1(k) = V_{\text{ref}}^* \\ & 0 \leq P_i^G(k) \quad \forall i \in \mathcal{N} \end{aligned}$$

and applies $P^G(k_0)$ to the P-generators of the microgrid.

III. Stability Analysis

In this section, we study the stability of the microgrid controlled by the three layer controller. First, we provide the controlled state space for the entire microgrid and proceed with deriving a numerical criterion for closed-loop stability.

A. MG in Network Variables

The dynamics of the entire DC microgrid can be obtained by interconnecting the dynamics of the lines (3), batteries (4) and damping elements (5), and by observing that $I_i = \sum_{j \in \mathcal{N}} B_{ij} I$ where $I = [I_1, \dots, I_M]$ is the current into the buses. The dynamics of the microgrid are given by

$$\dot{V} = C_t^{-1}\left(I_t + \text{diag}(V)^{-1} P^* - BI\right), \tag{14a}$$
$$\dot{I}_t = \alpha V + \beta I_t + S_B \gamma v + S_D \delta e + S_D \varepsilon q, \tag{14b}$$
$$\dot{v} = V_{\text{ref}}(V, I_t) - S_B^T V, \tag{14c}$$
$$\dot{e} = S_D^T I_t + \eta(S_D^T V - e), \tag{14d}$$
$$\dot{q} = S_D^T \text{diag}(V) I_t, \tag{14e}$$
$$\dot{I} = L^{-1} B^T V - L^{-1} R I, \tag{14f}$$

where

$$\begin{aligned} & C_t = \text{diag}(C_{t1}, \dots, C_{tN}), L = \text{diag}(L_1, \dots, L_M) \\ & S_B = \begin{bmatrix} \mathbf{I}_{N_B} \\ \mathbf{0}_{N_D \times N_B} \end{bmatrix}, S_D = \begin{bmatrix} \mathbf{0}_{N_B \times N_D} \\ \mathbf{I}_{N_D} \end{bmatrix}, \alpha = \text{diag}(\alpha_1, \dots, \alpha_N), \\ & \beta = \text{diag}(\beta, \dots, \beta_N), \gamma = \text{diag}(\gamma_1, \dots, \gamma_{N_B}), \\ & \delta = \text{diag}(\delta_{N_B+1}, \dots, \delta_{N_B+N_D}), \varepsilon = \text{diag}(\varepsilon_{N_B+1}, \dots, \varepsilon_{N_B+N_D}), \\ & \zeta = \text{diag}(\zeta_{N_B+1}, \dots, \zeta_{N_B+N_D}), \eta = \text{diag}(\eta_{N_B+1}, \dots, \eta_{N_B+N_D}), \end{aligned}$$

and $V_{\text{ref}}(V, I_t)$ implements either the time-variant (Def. 2) or the time-invariant (Def. 3) control law of the second layer controller. The actual P-injections at the busses are denoted by $P^* = [P_1^*, \dots, P_N^*]^T$ and P^* is a continuous function of time. In the following, the stability is investigated for the time-invariant version (13) of second layer controller.

B. Numerical Verification of Stability

In this subsection, we shift the variables to an arbitrary feasible equilibrium point and derive a numerical stability criterion which verifies asymptotic stability for the closed loop. We note that the steady state of (14) yields the power flow equation (2) which has in general more than one solution [20]. Because there are many potentially valid equilibria which are unknown, we define an arbitrary equilibrium point of (14) as

$$\overline{x} = \begin{bmatrix} \overline{V}^T & \overline{I}_t^T & \overline{v}^T & \overline{e}^T & \overline{q}^T & \overline{I}^T \end{bmatrix}^T$$

and define new error variables $\tilde{x} = x - \overline{x}$.

Proposition 1: For voltages $V_i > 0, i \in \mathcal{N}$, the system (14) with the time-invariant control law of Definition 3 can be represented in shifted variables by

$$\dot{\tilde{x}} = \underbrace{\begin{bmatrix} \tilde{A}_{11} & C_t^{-1} & 0 & 0 & 0 & -C_t^{-1} B \\ \alpha & \beta & S_B \gamma & S_D \delta & S_D \varepsilon & 0 \\ G_1 - S_B^T & G_2 & 0 & 0 & 0 & 0 \\ \eta S_D^T & \zeta S_D^T & 0 & -\eta & 0 & 0 \\ 0 & S_D^T \text{diag}(\tilde{V} + \overline{V}) & 0 & 0 & 0 & 0 \\ L^{-1} B^T & 0 & 0 & 0 & 0 & -L^{-1} R \end{bmatrix}}_{=: \tilde{A}(\tilde{V}, \overline{V}, P^*) \in \mathbb{R}^{\tilde{N} \times \tilde{N}}} \tilde{x}, \tag{15}$$

where $\tilde{A}_{11} = C_t^{-1}\text{diag}\left((\tilde{V}+\overline{V})\circ\overline{V}\right)^{-1}\text{diag}(P^*)$ and $\tilde{N} = 2N + N_B + 2N_D + M$.

Proof: Since $V_i > 0, \forall i \in \mathcal{N}$, the following steady-state values are obtained from (14):

$$\overline{I}_{ti} = 0\ \forall i \in \mathcal{N}_D, \overline{V}_i = V_{\text{ref},i}\ \forall i \in \mathcal{N}_B, \overline{e}_i = \overline{V}_i\ \forall i \in \mathcal{N}_D.$$

For the linear equations (14b), (14d) and (14f), the variable shift is trivial. The nonlinear equations (14a), (14e) result in

$$\begin{aligned} C_t\dot{\tilde{V}} &= \tilde{I}_t + \overline{I}_t + \text{diag}(\tilde{V}+\overline{V})^{-1}P^* - B(\tilde{I}+\overline{I}) \\ &= \tilde{I}_t + \text{diag}(\tilde{V}+\overline{V})^{-1}P^* - B\tilde{I} - \text{diag}(\overline{V})^{-1}P^* \\ &= \tilde{I}_t + \text{diag}\left((\tilde{V}+\overline{V})\circ\overline{V}\right)^{-1}\text{diag}(P^*)\tilde{V} - B\tilde{I}, \quad (16) \\ \dot{\tilde{q}} &= S_D^T\text{diag}(\tilde{V}+\overline{V})(\tilde{I}_t+\overline{I}_t) \quad (17) \\ &\overset{\overline{I}_t=0}{=} S_D^T\text{diag}(\tilde{V}+\overline{V})\tilde{I}_t. \quad (18) \end{aligned}$$

By using the time-invariant control law of Definition 3, the dynamics of $\dot{\tilde{v}}$ are given by

$$\begin{aligned} \dot{\tilde{v}} &= V_{\text{ref,lin}}(\tilde{V}+\overline{V}, \tilde{I}_t+\overline{I}_t) - S_B^T(\tilde{V}+\overline{V}) \\ &= (G_1 - S_B^T)\tilde{V} + G_2\tilde{I}_t + \underbrace{G_0 + G_1\overline{V} + G_2\overline{I}_t - S_B^T\overline{V}}_{=0}. \quad (19) \end{aligned}$$

The equation (15) can be obtained with (16), (17), (18) and (19). ■

Assumption 3: The feasible subspaces of voltage errors $\tilde{V}$, voltage equilibrium points $\overline{V}$ and P-injections P^* for safe operation are assumed as convex polytopes $\tilde{\mathcal{V}}, \overline{\mathcal{V}}$ and $\mathcal{P}$, which are described by the linear inequalities

$$\begin{aligned} \tilde{\mathcal{V}} &= \{\tilde{V} \in \mathbb{R}^N \mid a_j^T\tilde{V} \le 1, j = 1,\dots,N\}, \\ \overline{\mathcal{V}} &= \{\overline{V} \in \mathbb{R}^N \mid b_j^T\overline{V} \le 1, j = 1,\dots,N\}, \\ \mathcal{P} &= \{P^* \in \mathbb{R}^N \mid c_j^T P^* \le 1, j = 1,\dots,N\}. \end{aligned}$$

Theorem 2: Any equilibrium

$$\overline{x} \in \overline{\mathcal{X}} = \{\overline{x} \in \mathbb{R}^{\tilde{N}} \mid \begin{bmatrix}\mathbf{I}_N & \mathbf{0}_{N\times\tilde{N}-N}\end{bmatrix}\overline{x} = \overline{V} \in \overline{\mathcal{V}}\}$$

of the closed-loop system (15) is asymptotically stable for all $\tilde{V} \in \tilde{\mathcal{V}}, P^* \in \mathcal{P}$ if there exists a symmetric matrix $M \in \mathbb{R}^{\tilde{N}\times\tilde{N}}$ such that

$$M > 0 \quad (20)$$

$$\tilde{A}(\tilde{V},\overline{V},P^*)^T M + M\tilde{A}(\tilde{V},\overline{V},P^*) < 0 \quad (21)$$

is feasible for all $\tilde{V} \in \tilde{\mathcal{V}}, \overline{V} \in \overline{\mathcal{V}}$ and $P^* \in \mathcal{P}$.

Proof: Consider the Lyapunov candidate $V : \mathcal{D} \to \mathbb{R}, \tilde{x} \to \tilde{x}^T M\tilde{x}$ with

$$\mathcal{D} = \{\tilde{x} \in \mathbb{R}^{\tilde{N}} \mid \begin{bmatrix}\mathbf{I}_N & \mathbf{0}_{N\times\tilde{N}-N}\end{bmatrix}\tilde{x} = \tilde{V} \in \tilde{\mathcal{V}}\}.$$

The function V fulfills $V(0_{\tilde{N}}) = 0$ and $V(\tilde{x}) > 0$ in $\mathcal{D} - \{0\}$ since $M > 0$. Furthermore, $\dot{V}(\tilde{x}) = \tilde{x}^T(\tilde{A}^T M + M\tilde{A})\tilde{x} < 0$ is ensured in $\mathcal{D} - \{0\}$ by (21) [21, Theorem 3.7]. From [21, Theorem 3.3], it follows that the equilibrium points $\overline{x} \in \overline{\mathcal{X}}$ are asymptotically stable. ■

Remark 5: The conditions of Theorem 2 can be easily verified by solving a semi-definite program (SDP) with uncertain parameters $\tilde{V} \in \tilde{\mathcal{V}}, \overline{V} \in \overline{\mathcal{V}}$ and $P^* \in \mathcal{P}$ [22].

Remark 6: An ensured region of attraction of the equilibrium points $\overline{x}$ of Theorem 2 is given by the largest ellipsoid $\mathcal{E} = \{\tilde{x} \in \mathbb{R}^N \mid \tilde{x}^T M\tilde{x} \le c\}$ which is contained in the convex polytope $\tilde{\mathcal{V}}$ [21, Theorem 3.5].

The ellipsoid $\mathcal{E}$ is contained in $\tilde{\mathcal{V}}$ if and only if [23, Eq. 5.35]

$$\max\{a_j^T\tilde{x} \mid \tilde{x} \in \mathcal{E}\} \le 1 \quad \text{for} \quad j = 1,\dots,N.$$

IV. Simulation Results

In this section, we illustrate the stability and the power sharing of our three layer controller. We consider the meshed DC microgrid with $N = 5$ buses shown in Fig. 4. P-generators are placed at Buses 1 and 5, batteries are placed at Buses 1 and 2, P-loads are located at Buses 3 and 4, and damping elements are placed at Buses $3, 4$ and 5. The third layer controller generate values for P-generation P^G every $T = 2\,\text{s}$ and has a control horizon of $k_{\text{max}} = 2$ steps. The predicted constant loads during the sampling time T are

$$\begin{aligned} P_3^L(k = 1,\dots,5) &= \begin{bmatrix}10e3 & 10e3 & 10e3 & 18e3 & 10e3\end{bmatrix}\text{W}, \\ P_4^L(k = 1,\dots,5) &= \begin{bmatrix}8e3 & 5e3 & 8e3 & 10e3 & 8e3\end{bmatrix}\text{W}, \end{aligned}$$

where k indicates the time step. The P-generations produced by the third layer controller and the actual P-loads are shown in Fig. 5. Disturbances of $+1\,\text{kW}$ and $-1\,\text{kW}$ occur during the time spans $0.5\,\text{s}$ to $1.5\,\text{s}$ and $6.5\,\text{s}$ to $7.5\,\text{s}$, respectively, and are highlighted in gray in Fig. 5 and the following figures. These disturbances are not known by the third layer controller. The costs of the P-generators are $c(P_1^G) = 0.995P_1^G$ and $c(P_5^G) = P_5^G$. Because the cost of the power injection of Generator 1 is lower than Generator 5, generator P_1^G feeds more than twice the power P_5^G into the grid (see Fig. 5). The electrical parameters and control parameters of the microgrid are listed in Table I. The numerical values of

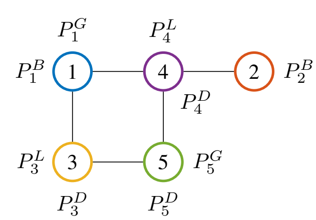

Fig. 4. Graph $\mathcal{G}(\mathcal{N},\mathcal{E})$ of the simulated DC microgrid with 5 buses

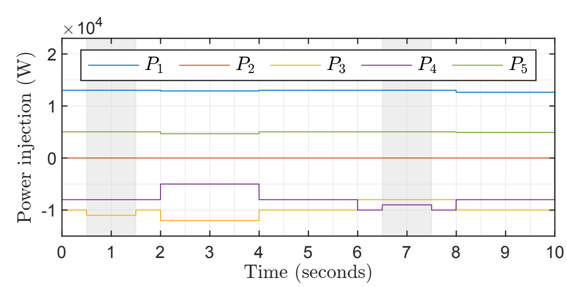

Fig. 5. Power injections by P-loads ($P_3 = P_3^L, P_4 = P_4^L$) and P-generators ($P_1 = P_1^G, P_5 = P_5^G$) at the five buses

TABLE I
PARAMETERS OF THE DC MICROGRID

Filter parameter	$R_{ti} = 0.2\,\Omega$	$L_{ti} = 2\,\mathrm{mH}$	$C_{fi} = 2\,\mathrm{mF}$
Line parameter	$R_l = 0.1\,\Omega$	$L_l = 2\,\mu\mathrm{H}$	$\frac{C_l}{2} = 20\,\mathrm{nF}$
Battery controller	$k_{1,i} = 0.5$	$k_{2,i} = 0.1$	$k_{3,i} = 50$
Damping controller	$k_{1,i} = 10$	$k_{2,i} = 20$	$k_{3,i} = 0.005$
	$\tau = 300$		

electrical parameters are based on [11, Appendix C]. The control law of the linearized second layer controller (13) around the operation point $V = 400 \cdot 1_N\mathrm{V}$ and $I_t = 0_N\mathrm{A}$ is given by

$$V_{\text{ref}} = \begin{bmatrix} V^*_{\text{ref}} \\ 400 \end{bmatrix} + \begin{bmatrix} 0 & 0 & 0 & 0 & 0 \\ -1 & 1 & 0 & 0 & 0 \end{bmatrix} V + \begin{bmatrix} 0 & 0 & 0 & 0 & 0 \\ \frac{7}{80} & -\frac{7}{80} & \frac{1}{16} & \frac{1}{80} & \frac{3}{80} \end{bmatrix} I_t, \tag{22}$$

where $V^*_{\text{ref}} = 400\,\mathrm{V}$. The voltages of the five busses are shown in Fig. 6. Because Bus 1 is the slack node, the voltage V_1 is controlled to V^*_{ref} The voltage V_2 is regulated by the second layer controller which for example increases the reference voltage $V_{\text{ref},2}$ during the disturbance from $0.5\,\mathrm{s}$ to $1.5\,\mathrm{s}$.

The power P^B and the performed work W^B of the batteries are shown in Fig. 7. Both batteries compensate the load disturbances from $0.5\,\mathrm{s}$ to $1.5\,\mathrm{s}$ and $6.5\,\mathrm{s}$ to $7.5\,\mathrm{s}$ and the desired equal power sharing is achieved. Furthermore, the batteries are (dis-)charged by the third layer controller during the time spans $2\,\mathrm{s}$ to $4\,\mathrm{s}$ and $8\,\mathrm{s}$ to $10\,\mathrm{s}$ such that the SOCs remain constant since the performed work W^B is zero after these time spans. The injected power P^D and consumed work W^D of the damping elements are shown in Figs. 8 and 9. The damping elements inject power when changes in the P-injections occur at the bus (see Fig. 5). Note that the damping elements do not consume energy due to the state q that ensures that the work done at steady state is zero (see Fig. 9). The conditions of Theorem 2 has been verified by solving an SDP with uncertain parameters (see Remark 5)

$$\tilde{V} \in \tilde{\mathcal{V}} = \{\tilde{V} \in \mathbb{R}^5 \mid -100 \le \tilde{V}_i \le 100\},$$
$$\overline{V} \in \overline{\mathcal{V}} = \{\overline{V} \in \mathbb{R}^5 \mid 350 \le \overline{V}_i \le 450\},$$
$$P^* \in \mathcal{P} = \{P^* \in \mathbb{R}^5 \mid -15000 \le P^*_i \le 15000\}.$$

Hence, any equilibrium $\overline{x} \in \overline{\mathcal{X}}$ of Theorem 2 is asymptotically stable.

The power sharing error $\Delta P^B = P^B_1 - P^B_2$ between the two batteries is plotted in a logarithmic scale in Fig. 10 for three different controllers in the second layer. The power sharing error of the time-invariant second layer controller of Definition 3 plotted in yellow shows an error around $\pm 2\,\mathrm{W}$ at steady state, e.g. at $t = 1.45\,\mathrm{s}$ and at $t = 7.45\,\mathrm{s}$. The controller of Definition 2 shown in red does not produce any steady-state error. To benchmark our second layer controllers, we replace the second level controller with a DC-OFP which finds the exact solution of (12) every $1\,\mathrm{ms}$. Note that this implementation is not real-time capable. Fig. 10 shows that the controller of Definition 2 achieves similar

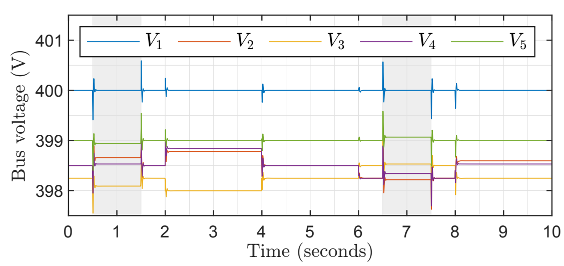

Fig. 6. Bus voltages over time

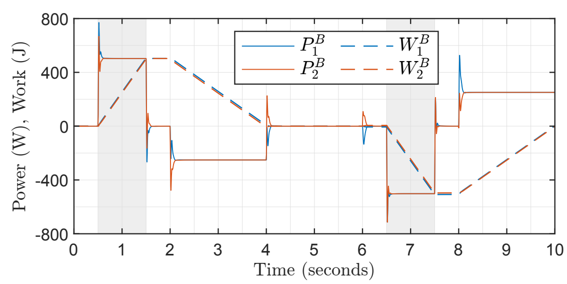

Fig. 7. Power and work of the two batteries over time

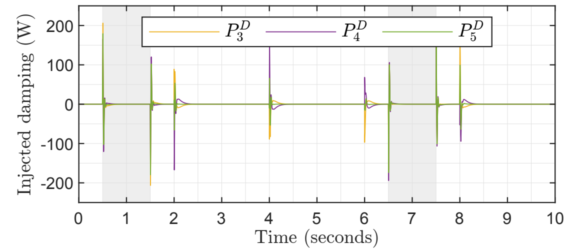

Fig. 8. Injected power of the three damping elements

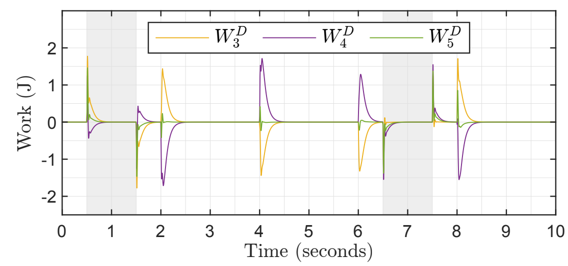

Fig. 9. Performed work of the three damping elements

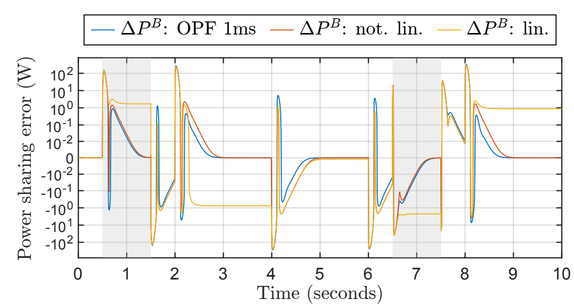

Fig. 10. Logarithmically scaled power sharing error $\Delta P^B = P^B_1 - P^B_2$ between the two batteries for the three different second layer controllers

performance compared to the DC-OPF with a maximum deviation between both sharing errors is $1\,\mathrm{W}$. Since all three second layer controllers generate voltage references for steady-state power sharing, it is worth comparing the steady-state power sharing errors. The power sharing error of the batteries at steady state $t = 1.45\,\mathrm{s}$ is shown in Table II for line resistances of $0.1\,\Omega$ and $1\,\Omega$. With higher line resistances, linearization errors have greater influence, because the microgrid operates further from the linearization point due to large voltage drops over the lines. The absolute power sharing errors at $t = 1.45\,\mathrm{s}$ are small compared to the losses of the network of 67.3W and 594.2W for $R_l = 0.1\,\Omega$ and $1\,\Omega$, respectively.

TABLE II

STEADY STATE POWER SHARING ERROR OF THE BATTERIES AT $t = 1.45\,\mathrm{s}$

Case	DC-OPF	2nd layer controller (8)	2nd layer controller (13)
$R_l = 0.1\Omega$	$\Delta P^B = 41$µW	$\Delta P^B = 62$µW	$\Delta P^B = 1.693$W
$R_l = 1\Omega$	$\Delta P^B = 142$µW	$\Delta P^B = -6.428$mW	$\Delta P^B = 11.60$W

V. CONCLUSION

In this paper, we proposed a hierarchical three layer controller that achieves economic dispatch, compensates load and generation disturbances with batteries performing power sharing, and stabilizes the power grid. In particular, we derived a novel control law for computing the voltages references for the batteries. Furthermore, we stabilized the microgrid containing P-generators and P-loads with voltage controllers for batteries and for active damping elements. In addition, we provided sufficient conditions for asymptotic stability. Future work includes the use of distributed optimization for the second layer controller, the consideration of flexible consumers for which the power consumption can be curtailed and the consideration of general ZIP-loads.

REFERENCES

[1] S. Homan, N. Mac Dowell, and S. Brown, "Grid frequency volatility in future low inertia scenarios: Challenges and mitigation options," *Applied Energy*, 2021.

[2] D. E. Olivares *et al.*, "Trends in microgrid control," *IEEE Transactions on Smart Grid*, no. 4, 2014.

[3] J. Schiffer *et al.*, "A survey on modeling of microgrids—from fundamental physics to phasors and voltage sources," *Automatica*, 2016.

[4] Y. E. García Vera, R. Dufo-López, and J. L. Bernal-Agustín, "Energy management in microgrids with renewable energy sources: A literature review," *Applied Sciences*, no. 18, 2019.

[5] H. Shayeghi *et al.*, "A survey on microgrid energy management considering flexible energy sources," *Energies*, no. 11, 2019.

[6] M. F. Zia, E. Elbouchikhi, and M. Benbouzid, "Microgrids energy management systems: A critical review on methods, solutions, and prospects," *Applied Energy*, 2018.

[7] X. Li and S. Wang, "A review on energy management, operation control and application methods for grid battery energy storage systems," *CSEE Journal of Power and Energy Systems*, 2019.

[8] F. Yang, X. Feng, and Z. Li, "Advanced microgrid energy management system for future sustainable and resilient power grid," *IEEE Trans. on Ind. Applicat.*, no. 6, 2019.

[9] J. Ferguson, M. Cucuzzella, and J. M. Scherpen, "Increasing the region of attraction in dc microgrids," *Automatica*, 2023.

[10] M. Cucuzzella, K. C. Kosaraju, and J. M. A. Scherpen, *Voltage control of DC networks: robustness for unknown ZIP-loads*. arXiv, 2019.

[11] M. Tucci *et al.*, "A decentralized scalable approach to voltage control of dc islanded microgrids," *IEEE Transactions on Control Systems Technology*, no. 6, 2016.

[12] P. Nahata *et al.*, "A passivity-based approach to voltage stabilization in dc microgrids with zip loads," *Automatica*, 2020.

[13] P. Nahata *et al.*, "Hierarchical control in islanded dc microgrids with flexible structures," *IEEE Transactions on Control Systems Technology*, no. 6, 2021.

[14] A. J. Malan *et al.*, *Passivity-based power sharing and voltage regulation in DC microgrids with unactuated buses*. arXiv, 2023.

[15] B. Fan *et al.*, "A consensus-based algorithm for power sharing and voltage regulation in dc microgrids," *IEEE Transactions on Industrial Informatics*, no. 6, 2020.

[16] C. de Persis, E. Weitenberg, and F. Dörfler, "A power consensus algorithm for dc microgrids," *IFAC-PapersOnLine*, no. 1, 2017.

[17] A. M. Kettner and M. Paolone, "On the properties of the power systems nodal admittance matrix," *IEEE Transactions on Power Systems*, no. 1, 2018.

[18] M. B. Cain, R. P. Oneill, and A. Castillo, "History of optimal power flow and formulations: Cain," *Federal Energy Regulatory Commission*, 2012.

[19] J. Machowski, J. W. Bialek, and J. R. Bumby, *Power system dynamics: Stability and control*, Rev. 2nd ed. Chichester: John Wiley & Sons Ltd, 2012.

[20] H. D. Nguyen and K. S. Turitsyn, "Appearance of multiple stable load flow solutions under power flow reversal conditions," *Power & Energy Society General Meeting*, 2014.

[21] H. K. Khalil, *Nonlinear control*. Boston: Pearson, 2015.

[22] S. P. Boyd and L. Vandenberghe, *Convex optimization*. Cambridge UK and New York: Cambridge University Press, 2004.

[23] S. P. Boyd *et al.*, *Linear matrix inequalities in system and control theory*. Philadelphia: Society for Industrial and Applied Mathematics, 1994.